SPECTRUM OF ENGINEERING SCIENCES
ISSN (E) 3007-3138 (P) 3007-312X VOLUME 4, ISSUE 3, 2026

APPLICATION OF AN AI MODEL: DEEP NEURAL NETWORKS WITH BAYESIAN OPTIMIZATION FOR PREDICTION OF SUBGRADE RESILIENT MODULUS

Rawid Khan[*1], Sahibzada Hamza Jan[2], Fawad Mehmood[3], Muhammad Atif Hussain[4]

[*1,2,34]*Department of Civil Engineering University of Engineering and Technology Peshawar Peshawar, Pakistan*

[*1]dr.rawid@uetpeshawar.edu.pk, , [2]shamzajan@uetpeshawar.edu.pk, [3]17pwciv4843@uetpeshawar.edu.pk, [4]muhammadatif@uetpeshawar.edu.pk

DOI: https://doi.org/10.5281/zenodo.22706360

Keywords
Resilient Modulus, Subgrade Soil, Artificial Neural Network, Deep Neural Network, Bayesian Optimization, Machine Learning, Pavement Engineering

Article History
Received: 01 January 2026
Accepted: 16 March 2026
Published: 31 March 2026

Corresponding Author: *
Rawid Khan

Abstract
The resilient modulus (Mr) of subgrade is an important parameter in pavement structural design because it characterizes the subgrade under repeated vehicular traffic loading. It impacts pavement design life, layer thickness, economy, distress, and rehabilitation. Determination of Mr in the laboratory through repeated load triaxial test (RLTT) is considered the most reliable method; however, it is time-consuming, expensive, equipment-intensive, and requires expert personnel. Additionally, to overcome the RLTT limitations, widely used California Bearing Ratio (CBR)-based Mr–CBR correlations are often unreliable. Recently, machine learning (ML) techniques, like Artificial Neural Networks (ANNs), have been used to predict subgrade Mr using basic soil properties and stress state variables. However, manual trial-and-error tuning of ANN hyperparameters can be time-consuming and may overlook optimal configurations. This study used a dataset from literature containing 995 processed data points of A-4, A-6, and A-7-6 soils, with their Atterberg limits, dry density (DD), moisture content (MC), percent passing No. 200 sieve (P#200), and stress state variables, as model inputs to predict subgrade Mr using a Deep Neural Network (DNN) with hyperparameters optimized via Bayesian Optimization (BO). The BO framework included six (6) tunable hyperparameters. The optimized DNN showed strong performance, achieving R^2 values greater than 0.90 for training and validation sets, and 0.85 for the testing set, with corresponding MAE and MAPE values below 2.6 MPa and 10%, respectively. Sensitivity analysis showed that plasticity index (PI), deviator stress (σd) and MC were the most influential, while DD showed minimal influence on subgrade Mr prediction.

INTRODUCTION

In the field of transportation engineering, pavement degradation is a recurring problem. When subjected to repeated traffic loads, pavements can develop different distresses, including ruts, cracks, potholes, and permanent deformation. The performance and service life of flexible pavements depend on the behavior and stiffness of the soil underneath the pavement, which is known as the subgrade soil [1]. The required thickness and material specifications of the pavement layers above the subgrade are affected by the subgrade's stiffness [2]. Subgrade soils are usually evaluated using the conventional California Bearing Ratio (CBR) test, however, CBR being a quasi-static property, cannot adequately represent the behavior of pavement structures as well as the strain-stress behavior of soils during repeated wheel loading [2], [3], because under such repeated loading conditions subgrade response is considered pseudo-elastic [4]. Subgrade materials subjected to cyclic loading typically exhibit both resilient and permanent deformation, and shakedown theory is often used to characterize this behavior [5]. As a result, to better depict stress situations, the American Association of State Highway and Transportation Officials (AASHTO) recommends using Mr in the Mechanistic Empirical Pavement Design Guide (MEPDG). This improves the accuracy of pavement performance prediction, as well as the ability to compute layer thicknesses and anticipate how pavement layers would react under traffic loads. Therefore, correct estimation of subgrade resilient modulus is important [2], [6].

Pavement materials under repeated loading exhibit stress-strain behavior which is explained in terms of its resilient modulus [7]. In pavement materials as well as for the critical subgrade layer, the resilient modulus measures stiffness rather than strength, reflecting the ability of the material to sustain traffic loads with minimal recoverable deformation [8]. Hveem was the first who discovered that unbound granular materials deform elastically under transient load, implying that the deformation is reversible. A more realistic understanding of the resilient modulus was later established by Seed et al., who defined it as the ratio of deviator stress to recoverable strain. Equation (1) shows that Mr is expressed as cyclic deviatoric stress (σ_d) divided by recoverable axial strain (ε_r), where σ_d is the difference between major and minor principal stresses (σ_1 and σ_3) [9].

$$Mr = \frac{\sigma_d}{\varepsilon_r} \qquad (1)$$

In the laboratory, Mr is obtained via the repeated load triaxial test (RLTT), which exerts a steady cell pressure along with a cyclic deviator stress, subsequently measuring the resilient axial strain. RLTT is the most commonly recognized method to obtain Mr. During the test, the sample is enclosed in a cylindrical chamber including a thin membrane, and lateral confining pressure (σ_3) is exerted from the sides through that membrane. An axial pressure (σ_1) is then applied multiple times, with pauses and unloading phases in between, in order to replicate the traffic loads from vehicles. Deformations are recorded, and the change in specimen length is noted in every cycle. However, laboratory assessment of Mr has limitations: it is time-consuming, necessitates numerous samples and expert technicians, and requires costly equipment [10], [11], [12], [13]. Figure 1 depicts the schematic diagram of the mechanical behavior of unbound aggregates subjected to triaxial testing and the stresses applied.

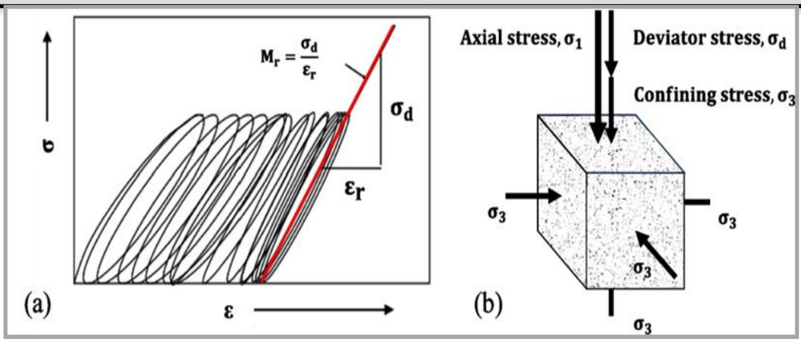

Figure 1: (a) Behavior of unbound materials during triaxial testing; (b) Applied stresses during triaxial testing. Adopted from [13].

Furthermore, the resilient modulus of subgrade soils is a variable property rather than a constant one. It varies with stress factors, moisture levels, soil composition, and the manner in which the load is applied [1]. Atterberg limits, optimal moisture content, and maximum dry density all have an impact. Coarser soils typically have higher Mr values. Soils with a high liquid limit and plasticity index typically produce lower Mr. Resilient modulus increases with density and particle size [1]. Previous studies have indicated that various factors are significant for fine-grained compared to granular soils. In fine-grained soils, water content, compaction, stress level, and variations in density post-compaction are all significant factors. For granular soils, the essential factors vary. Confining pressure, load frequency, void ratio, saturation degree, and the quantity of fines passing sieve No. 200 are more significant [6]. Multiple studies have verified that stress state and moisture are two major factors influencing resilient modulus behavior [14].

Considering both time and cost tradeoffs involved with laboratory testing of Mr, instead, it is usually convenient to use prediction models to determine Mr. As a result, scientists have created empirical and regression-based models to predict Mr using soil properties and stress conditions [6]. Nonetheless, these models come with their own limitations. They are often developed for specific materials and may not perform effectively for all types of soils because of the intricate, nonlinear characteristics of subgrade soils [6],[11].

CBR testing is well-established and has existed for many years, but it's overly empirical. This is why it is not effective for mechanistic empirical design [12]. Earlier research indicates that varying Mr–CBR correlations can lead to significantly different pavement design results and directly affect the necessary thickness of unbound granular layers. Certain correlations might result in uneconomical designs because of overly thick layers or increased material quality requirements. Thus, choosing a suitable MR–CBR correlation is heavily influenced by soil type and is crucial for obtaining dependable and cost-effective pavement design [15].

Instead of expensive, complicated lab testing, using artificial intelligence (AI) for predicting Mr is a better alternative [3], [16]. AI methods can be used to predict resilient modulus using basic soil properties [17], [18]. Machine learning (ML) is a subset of AI [19]. By using ML, computers can identify patterns from data, and then predict patterns, without having to be explicitly programmed for each task. Due to the increasing availability of computational power and large datasets, ML techniques have been increasingly applied in engineering and geotechnical applications [20]. As an alternative to traditional methods, machine learning (ML) techniques have gained interest due to their capability to model intricate nonlinear connections between soil characteristics and pavement behavior, and previous studies have shown that ML techniques can be effectively applied to the prediction of resilient modulus. [6], [20].

AI encompasses different methods like Artificial Neural Networks (ANNs), Random Forest (RF), and Support Vector Machines (SVM), among many others [19]. These are all smart computational tools that can be leveraged to analyze how materials respond to different types of stress-strain and loading conditions [21]. Furthermore, among all machine learning methods, ANNs are the most common in geotechnical engineering [19]. ANNs are highly effective for predicting resilient modulus. This is due to their ability to manage intricate, non-linear relationships among soil characteristics, stress conditions, and pavement behavior. Research indicates that ANNs frequently outperform traditional regression-based techniques [22].

While ANN models excel at predicting the resilient modulus, their effectiveness significantly relies on selecting appropriate configurations for the network and its hyperparameters [23], [24]. Many previous studies selected those settings manually, experimenting with various values until they found a successful result. This requires significant computational time and does not consistently yield optimal outcomes [25], [26]. As a result, advanced optimization approaches such as Bayesian Optimization (BO) are increasingly being explored to improve machine learning-based resilient modulus prediction models through efficient hyperparameter tuning [27]. This study builds a Bayesian Optimization (BO) based Deep Neural Network (BO-DNN) to predict the resilient modulus of A 6, A 7 6, and A 4 subgrade soils. The model takes soil index properties, stress state variables, and AASHTO soil classifications as inputs. Before building the model, outliers were removed, data was normalized, soil classes were one hot encoded, and the dataset was split in a balanced and stratified manner. Bayesian Optimization was then used to automatically tune and select the best DNN settings by lowering the validation error. Finally, the model's predictions and behavior were analyzed using several statistical measures, residual analysis, and sensitivity analysis.

Literature Review

Numerous recent research efforts have employed ANNs to estimate resilient modulus. According to [20], approximately 50% of machine learning models designed to forecast resilient modulus utilize ANNs. ANNs have also been employed in geotechnical engineering for quite some time now [28]. This illustrates the significance of ANNs in geotechnical and pavement engineering. The research by [1] utilized an ANN to predict resilient modulus based on soil characteristics such as liquid limit, plasticity index, moisture content, and dry density. The researchers used data from cyclic triaxial testing and Ultrasonic Pulse Velocity (UPV) with ANN modeling. Their findings indicated that the ANN model closely aligned with the resilient modulus values measured experimentally. The accuracy of predictions, assessed using Pearson's correlation, exceeded 85% across all test sets. This demonstrates that ANN methods can effectively and reliably predict resilient modulus.

Another research developed an ANN model to estimate the resilient modulus of silty subgrade soils. Water content, density ratio, and octahedral shear stress were utilized as input variables. Their ANN model demonstrated high accuracy, achieving an R^2 value close to 0.99. This indicates that ANN methods are effective in modeling resilient modulus across various moisture and stress scenarios. The research additionally discovered that water content is a key factor influencing resilient modulus [14]. Another recent study [29] evaluated three machine learning models, including ANN, Multi-Expression Programming (MEP), and Genetic Expression Programming (GEP) for predicting resilient modulus. A vast database of subgrade soils and stress-state variables was employed. All three models made accurate predictions, but the GEP model excelled the most. Nonetheless, the ANN model performed admirably, achieving training and testing R^2 values of 95% or greater. The research additionally identified that dry density, confining stress, moisture content, and plasticity index are key elements affecting resilient modulus behavior. Similar research was conducted by [22], where an extensive dataset with 1,683 resilient modulus datapoints along with ANN modeling was utilized for predicting Mr of both sticky (cohesive) and non-sticky (non-cohesive) soils. The ANN model incorporated input elements like soil gradation, plasticity index, density, saturation ratio, and stress state variables. The ANN model performed exceptionally, achieving an R^2 value close to 0.96. A sensitivity analysis indicated that the key factors influencing resilient modulus were saturation ratio, deviator stress, and the quantity of fine particles in the soil [22]. Even visual-manual soil classification indicators alongside stress-state variables have been employed basic as inputs alongside ANN modeling to estimate the resilient modulus of subgrade soils [10]. The research utilized a substantial database of 1,308 soil samples and experimented with around 2,000 various ANN configurations to determine the optimal network architecture. Their ultimate ANN model achieved impressive results, exhibiting a correlation coefficient near 0.96 [10]. This indicates that ANN methods can provide dependable and inexpensive assessments of resilient modulus by utilizing only straightforward, field-based soil descriptions.

Additionally, although there is limited research on this topic, some prior studies have effectively utilized ANN models to forecast the resilient modulus of recycled and chemically treated pavement materials. These investigations examined substances such as recycled concrete aggregates, reclaimed masonry materials, geopolymer-treated soils, and waste from construction and demolition. Using ANN for predicting resilient modulus stabilized with additives like lime, cement, fly ash, cement fly ash (CFA), and cement kiln dust (CKD) has also been examined. Nearly all of these research efforts yielded reliable predictive outcomes. The majority of ANN-based models demonstrated R^2 values (the coefficient of determination) equal to or exceeding 0.90. These results demonstrate once more that ANN methods effectively model complex resilient modulus behavior for various pavement material types [20], [30], [31]. Another recent study [32] researched with an attempt to predict Mr of expansive soils stabilized with apricot kernel shell ash. The ANN model achieved impressive results, with an R^2 value of approximately 0.96 and achieved better performance than multiple regression [32]. This indicates that ANN methods can be utilized to assess the resilient modulus of stabilized subgrade materials. A one of kind study found that adding 6-9% waste paper sludge (WPS) significantly increased the resilience modulus (Mr) of expansive subgrade soils. They developed ANN models to predict Mr, achieving excellent accuracy with R^2 ranging from 0.95 to 0.99, exceeding typical regression techniques with R^2 ranging from 0.87 to 0.89. Microstructural examination and simulations confirmed the improvement. The study concludes that ANN models provide a precise, effective alternative to lengthy lab testing [33].

Deep Neural Network (DNN) have also been used for predicting Mr. For example, a recent study employed Deep Neural Network algorithms for predicting resilient modulus by utilizing an extensive database of both coarse and fine soils obtained from the Long-Term Pavement Performance (LTPP) database. The study attained coefficients of determination (R^2) exceeding 0.99 [34]. Furthermore, work has been done on developing a Deep Neural Network (DNN) model to forecast the resilient modulus of compacted subgrade soils in varying moisture and freeze-thaw scenarios [35]. The study employed soil index properties and stress-state variables as inputs. Their DNN model outperformed various standard machine learning techniques and achieved a high testing R^2 value nearing 0.98 [35]. Another study assessed various machine learning techniques to forecast the resilient modulus of three subgrade soil including A-4, A-6, and A-7-6, by utilizing data from repeated load triaxial tests along with stress-state variables. Among all the models the study evaluated, the Deep Neural Network (DNN) performed the best. It attained validation R^2 values exceeding 0.99 and surpassed numerous conventional machine learning and regression techniques [36]. A vast number of other researchers have effectively employed ANNs in diverse manner for predicting resilient modulus for pavement design, and have attained excellent model performance in many studies [20].

In recent times Bayesian Optimization (BO) has been increasingly used in civil, pavement, and geotechnical engineering to enhance machine learning model efficacy via effective hyperparameter tuning. Previous studies have effectively integrated BO with ANN, DNN, XGBoost, SVR, and ensemble learning models among many others to forecast pavement performance, asphalt mixture characteristics, concrete compressive strength, including high performance concrete, subgrade resilient modulus, and geotechnical material properties [26], [37–49]. Studies indicated that Bayesian Optimization facilitated a more effective and organized approach to hyperparameter tuning [26], [40], [38], enhancing prediction performance in contrast to traditional tuning techniques like manual trial-and-error and grid search [40]. The basic working mechanism of the Bayesian optimization process is shown in Figure 2.

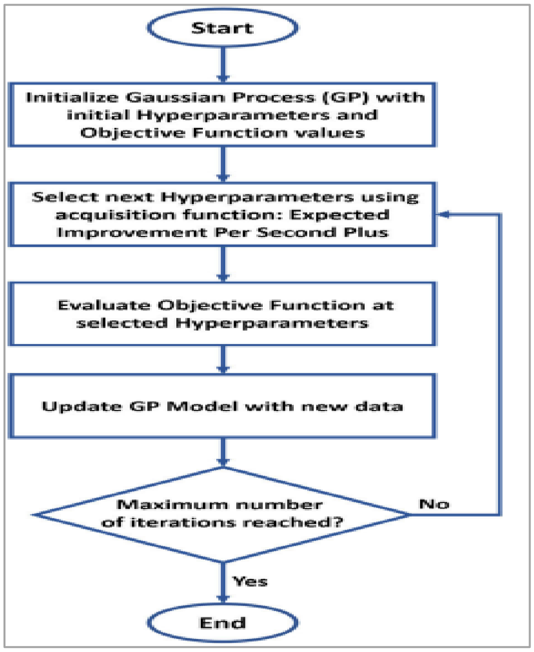

Figure 2: Bayesian optimization mechanism flow chart. Adapted from [50].

METHODOLOGY

The entire preprocessing pipeline of this study, along with the implementation of Bayesian optimization (BO) and post-hoc analysis of the obtained ANN model, was conducted in MATLAB. The entire pipeline was ensured to be reproducible through the use of a fixed random seed at key locations.

A. Data Collection

The dataset used in this study was obtained from recently published literature [11]. The original Excel file of the dataset contained approximately 1050 data points, comprising several variables related to soil classification, physical properties, and stress conditions. However, only the most relevant variables were retained before starting preprocessing. These include AASHTO soil classification, liquid limit (LL), plastic limit (PL), plasticity index (PI), moisture content (MC), dry density (DD), percent passing No. 200 sieve (P#200), confining stress (σ_3), and deviatoric stress (σ_d). The remaining variables were omitted to maintain model simplicity and avoid redundant information. The resilient modulus (Mr) column was considered the target or output variable of the dataset.

B. Outlier Removal

According to good machine learning practices, the dataset was first randomly shuffled to ensure randomness and remove any prior bias or patterns present within it. Next, outliers were detected using the Interquartile Range (IQR) method, which was applied only to the target variable, resilient modulus (Mr). The lower and upper bounds were defined by Equation (2):

$$Q_1 - 1.5 \times IQR \leq x \leq Q_3 + 1.5 \times IQR \quad (2)$$

where Q1 and Q3 are the first and third quartiles, and IQR is the interquartile range, which is defined by Equation (3):

$$IQR = Q_3 - Q_1 \quad (3)$$

Any data points falling outside the range defined in Equation (2) were flagged as outliers and were removed to make the data more consistent and reduce noise.

C. Data Preprocessing Validation

A statistical summary table of the raw and cleaned dataset was generated to assess data quality. Histograms and side by side boxplots of the target variable Mr were also generated to assess its data distribution before and after outlier removal. A preliminary correlation analysis was also performed to examine relationships between input variables through developing a correlation heatmap.

D. Categorical One-Hot Encoding

Categorical soil types (A-4, A-6, and A-7-6) were converted into numerical form using one hot encoding. This process creates binary variables for each soil class, allowing the model to interpret categorical information without introducing ordinal bias. This step simply makes it easy for the ANN model to recognize the soil type or classification within a certain row by checking if the value for a certain soil is 0 or 1. In simple terms, the process develops an extra binary indicator column for each soil type within each datapoint. A value of one (1) is placed in the column corresponding to the soil type present, while the other soil columns receive a value of zero (0).

E. Target-Based Stratified Dataset Splitting

The cleaned dataset was split into training, validation, and testing subsets using a combined stratification approach to preserve both soil type distribution and target value distribution across subsets. The process involved, grouping the Mr values into ten (10) bins of equal width. Then, each data point was labeled by combining its soil type with its Mr bin. Within each of these combined groups, 60% of the samples were randomly assigned to training, 20% to validation, and 20% to testing. This way, all three subsets ended up with similar mixtures of soil types and Mr ranges, avoiding any unfair bias. Tables showing the mean and standard deviation, along with the proportion of data points of each soil

F. *Data Normalization*

All input features and the target variable were scaled to the [0, 1] range using minimum-maximum normalization. For any input variable, its value x is normalized as x_{norm} using Equation (4), where x_{min} and x_{max} are the minimum and maximum values of that variable, respectively.

$$x_{norm} = \frac{x - x_{min}}{x_{max} - x_{min}} \quad (4)$$

To avoid data leakage during normalization, the minimum (x_{min}) and maximum (x_{max}) values were obtained from the training set only, and the same numbers were then used to scale the validation and test sets. Normalizing data prevents any variable with naturally larger numbers from taking over the training process.

G. Development of Deep Neural Network (DNN) using Bayesian Optimization (BO)

In this study, Bayesian optimization (BO) was used to automatically determine the optimal network configuration, avoiding manual trial-and-error selection. The optimization was implemented using MATLAB's bayesopt function.

Artificial neural networks, or ANNs, are a type of machine learning model inspired by the structure and operation of the human brain. An artificial neural network (ANN) is made up of linked neurons stacked in layers, including an input layer, one or more hidden layers, and an output layer. Each neuron receives some input, analyzes it via weighted connections and an activation function, and then sends the output to the next layer [1], [19]. To be more specific, each neuron computes a weighted sum of its inputs before applying a nonlinear activation function to generate an output. Biases are also used to change the activation function, giving the network greater flexibility [11]. While the network undergoes training, it continuously modifies its weights and biases to reduce prediction error and improve its accuracy in making predictions. Due to their ability to learn intricate, nonlinear patterns directly from data, ANNs are often used for regression and prediction problems where it's hard to write down a conventional mathematical relationship [1], [19]. In a feedforward ANN, data moves solely in one direction, meaning from the input layer across the hidden layers and finally to the output layer, without any feedback loops. The concealed layers perform the primary computations and extract patterns from the input variables, while the output layer delivers the ultimate prediction. A diagram of the feedforward ANN configuration utilized in this study is presented in Figure 3. In the feedforward phase, the anticipated output is evaluated against the target output, and the prediction error is determined. The error is then transmitted back through the network employing the backpropagation method, with continual adjustments made to the weights and biases to decrease the error and enhance the model's performance [1], [19].

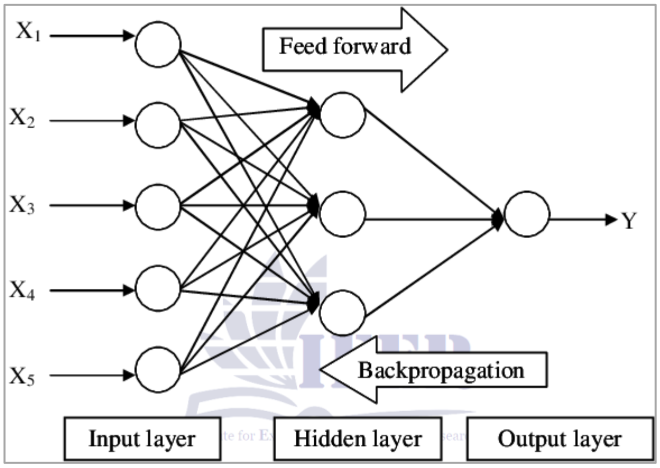

Figure 3: Architecture of a typical multilayer feed-forward neural network. Adapted from [51]

Deep learning (DL) is a more sophisticated area of machine learning, employing deep neural networks (DNNs), also known as ANN models with multiple hidden layers. The more complex structure of DNNs can model nonlinear relationships and interactions in large datasets more effectively than regular shallow ANNs. The feedforward DNN architecture was adopted to model the nonlinear relationships between soil properties, the stress state variables, and resilient modulus values in this study [19].

Some limitations are also associated with the standard ANN models. They are sometimes referred to as "black boxes" because they are not possible to observe how they make predictions. Also, they don't provide an easy to use equation for engineers. They are known to be data hungry models and with small quantities of data, they fall short of generalizing well. Another problem is that ANNs do not obey real physics, because they learn patterns of numbers and there are no soil mechanics rules behind them. Finally, trained ANN are only valid for the range of input values with which they were trained. The predictions may be less precise if used outside of the range [52].

In machine learning and deep learning models, Bayesian optimization, or BO, is a sequential approach that effectively adjusts hyperparameters. The decisions regarding ANNs or DNNs, such as the quantity of hidden layers, neurons, learning rate, activation functions, and training iterations, can significantly influence the prediction accuracy and the model's ability to generalize [24]. BO explores the hyperparameter space more systematically than grid search, random search, or trial-and-error methods. BO builds a probabilistic model (a surrogate) of the objective function and keeps updating that model with results from earlier evaluations [27], [53]

When BO is run, it uses an acquisition function to decide the next hyperparameter combinations to evaluate. The goal is to prioritize settings that might improve performance and to avoid those that are not likely to help [54], [55]. Because of this, BO can be more efficient than standard tuning methods, as it can find near-optimal configurations with less computation [26], [56]. This is very relevant in the case of DNNs, where hyperparameters play a decisive role in the prediction accuracy, convergence in training, and general stability of the model [57], [58], [59]. In addition to this, some studies have found that using BO-based tuning reduces the cost of manual hyperparameter tuning while improving accuracy and robustness [59], [60], [61].

Inside the BO framework, a feedforward DNN architecture was adopted, consisting of an input layer, multiple hidden layers, and a single output neuron with linear activation for regression. The tunable hyperparameters of the DNN and their ranges, which were programmed into BO, along with the BO settings are presented in Table I.

Table I. Bayesian Optimization Settings and Tunable Hyperparameters Of the DNN Model

Hyperparameter	Range / Options
Number of hidden layers	1 – 5
Number of neurons per layer	10 – 30
Activation function	ReLU, tanh, sigmoid, leaky ReLU
Optimizer	Adam, SGDM, RMSProp
Initial learning rate	10^{-4} – 10^{-2} (log scale)
Maximum training epochs	50 – 3000
Acquisition function	Expected Improvement (EI)
Random Iterations or Trials	20
Guided Iterations or Trials	80

For each iteration of the optimization process, the BO built a DNN using a specific set of hyperparameters from the available ranges, trained it on the training data, and evaluated its performance on the validation data. The objective function of the BO was configured to minimize the validation MAE, and its goal was to achieve the lowest possible Mean Absolute Error (MAE) on the validation set within a fixed number of trials.

The BO ran for 100 trials in total. The first 20 trials were completely random, focusing on exploration rather than exploitation of the available hyperparameter space. After that, the search was guided by the Expected Improvement (EI) acquisition function, further exploiting the more promising regions of the hyperparameter space. The BO was configured in such a way that, inside each BO trial, training stopped early if the validation error did not improve for 15 consecutive checks. This saved time and prevented overfitting.

For every trial, training, validation, and testing performance was tracked. The BO process was solely driven by the validation MAE as the objective function, and the test MAE was only monitored and played no part in the BO process itself. After training, predictions were denormalized back to original Mr units (MPa) for every evaluation, and model performance within that trial was evaluated on training, validation, and test sets using metrics such as Mean Absolute Error (MAE), Root Mean Square Error (RMSE), Coefficient of Determination (R^2) and Mean Absolute Percentage Error (MAPE). The above-mentioned metrics are defined in Equations (5) – (8), where y_i and $\hat{y}_i$ represent the actual and predicted values, respectively, and is the number of samples.

$$MAE = \frac{1}{n}\sum_{i=1}^{n}|y_i - \hat{y}_i| \quad (5)$$

$$RMSE = \sqrt{\frac{1}{n}\sum_{i=1}^{n}(y_i - \hat{y}_i)^2} \quad (6)$$

$$R^2 = 1 - \frac{\sum_{i=1}^{n}(y_i - \hat{y}_i)^2}{\sum_{i=1}^{n}(y_i - \bar{y})^2} \quad (7)$$

$$MAPE = \frac{100}{n}\sum_{i=1}^{n}\left|\frac{y_i - \hat{y}_i}{y_i}\right| \quad (8)$$

The BO process consistently tracks the DNN model with the lowest objective function (validation MAE), along with its corresponding hyperparameters, and constantly updates the best model, as well as the BO's internal surrogate model. The BO was coded to save the DNN model with the lowest objective function (validation MAE) to a .mat file at the end of the trials. The .mat file contained the trained network, its training history, convergence history, hyperparameter settings, total network training time, the performance and error metrics for all three datasets (training, validation, and test), and the random number generator state. The BO mechanism utilized within this study is illustrated in Figure 4.
Additionally, a log file in the form of a .mat file containing details of each trial evaluation was saved. Furthermore, for each trial evaluation, the predicted and actual Mr values of each datapoint, along with the corresponding information about the data point's input variable values, were saved to separate individual .mat files.
The BO code was set up to generate MATLAB bayesopt's inherent plot, displaying how the minimum objective value changes as the function evaluations progress. After the optimization finished, using the saved .mat log file, additional plots were developed, showing how each metric (MAE, RMSE, R^2, MAPE, MSE) changed over all 100 trials, and the trial with the lowest validation MAE was clearly marked on the plots.

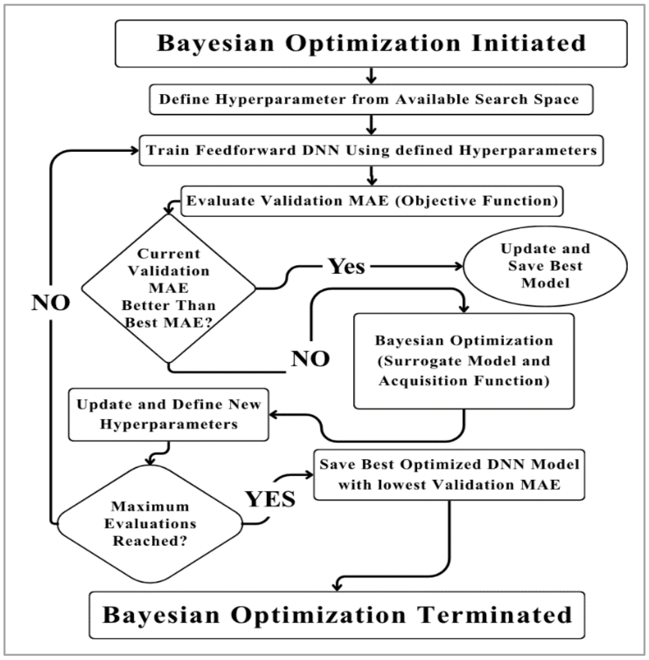

Figure 4: Flowchart of the Bayesian optimization process for DNN hyperparameter tuning.

H. DNN Model Architecture, Performance, and Residual Analysis

First, a schematic of the selected DNN was generated to show its architecture, including neurons and the interconnected layers. Using the .mat file containing the predicted and actual Mr values of the selected DNN model, the performance and error of the optimized DNN model were evaluated at both the global level (entire subsets) and at the soil-specific level (A-4, A-6, and A-7-6), and the corresponding results were

summarized in a tabulated form using standard performance metrics. Scatter plots of predicted versus actual resilient modulus (Mr) were generated for the training, validation, and test sets to visualize the predictive accuracy of the DNN model
across the actual Mr range. A diagonal line was added to show where perfect predictions would fall, and key metrics like R^2, RMSE, MAE, and MAPE were displayed on each subplot of the corresponding subset. Using the training history from the saved .mat file of the DNN model, the training loss and validation loss were plotted against the number of iterations to see how the model learned over time
and to find where it stopped improving (early stopping).
The residuals (prediction errors) from only the test set were also analyzed to understand how they behaved against predicted values and across different soil types to verify whether the model worked consistently for each soil class. The absolute error distribution was also plotted using a histogram to examine the largest errors more closely. Lastly, the mean absolute error (MAE) for each soil type was plotted and compared to assess how model performance varied across different soil classes.

I. Sensitivity Analysis

A parametric sensitivity was conducted to analyze how much each continuous input variable changes the predicted Mr. Only continuous input variables were varied during sensitivity analysis, while the soil type was kept fixed at a constant soil condition. The process involved taking each input variable one at a time and varying it from its smallest value to its largest value using only the training data, while keeping all other variables at their average values. The sensitivity percentage for each variable is then obtained by using (9), where $\hat{y}_{max}$ and $\hat{y}_{min}$ are the predicted outputs at the maximum and minimum values of the input variable, respectively and $\hat{y}_{\text{base}}$ is the model prediction at the mean values of all variables.

$$Sensitivity(\%) = \frac{|\hat{y}_{max} - \hat{y}_{min}|}{\hat{y}_{\text{base}}} \times 100 \quad (9)$$

Equation (9) calculates the degree to which a prediction changes when varying that variable from its minimum to its maximum value, as compared to the prediction at the average values. This process identifies which inputs matter the most in regard to their impact on model output prediction. A bar chart was also generated for easy visual analysis and comparison of the parametric sensitivity of each input variable.

J. Instructions on the use and limitations of the model

This section includes instructions and directions regarding the use of the DNN model for predicting subgrade Mr using new input data. Limitations associated with the DNN model are also included in this section.

RESULTS

K. Data Distribution and Preprocessing Results

Table II presents the statistical summary of the unprocessed and processed datasets. Table III shows the detailed statistics of outliers removed from each soil group. The Interquartile Range (IQR) method flagged and removed a total of 40 Mr datapoints. The processed dataset consisted of 995 data points. It can be observed that most input variables remained largely unchanged after preprocessing, since outlier removal was applied only to the target variable, the resilient modulus (Mr).
Input variables of the processed dataset exhibited patterns similar to those expected from laboratory data. The skewness of the input variables after outlier removal remains almost normal to moderate. The kurtosis values ranged from 1.54 to 3.87, with most variables exhibiting a normal distribution. Some variables, like confining stress and deviatoric stress, are more spread out and have fewer extreme values, while others, like MC and DD, have a few more extreme values than usual. Overall, based on skewness and kurtosis, the input data does not show severe non-normality or extreme outliers.

Table II. Statistical summary of raw and processed datasets.

Input Variables	Raw Dataset					Processed Dataset				
	Min	*Max*	*Std*	*Skewness*	*Kurtosis*	*Min*	*Max*	*Std*	*Skewness*	*Kurtosis*
LL	21.6	63.3	9.26	0.26	2.58	21.6	63.3	9.25	0.27	2.6
PL	12	28.2	2.92	0.03	3.4	12	28.2	2.92	0.04	3.47
PI	6.4	43	7.8	0.46	2.76	6.4	43	7.83	0.46	2.76
MC (%)	14.9	36.5	3.97	0.57	3.83	14.9	36.5	3.92	0.58	3.87
DD (kN/m^3)	12.76	19.12	1.13	0.16	3.71	12.76	19.12	1.11	0.13	3.78
P#200 (%)	38.6	99.1	14.8	-0.55	2.64	38.6	99.1	14.91	-0.56	2.63
σ_3 (KPa)	12.94	45.88	11.42	0	1.53	12.94	45.88	11.39	0.04	1.54
σ_d (KPa)	10.55	69.29	18.99	0.02	1.71	10.55	69.29	18.75	-0.03	1.74
Mr (MPa)	9.9	72.91	11.2	1.09	4.1	9.9	52.65	9.37	0.68	2.82

Table III. Number of outliers removed from each soil category.

Soil Type	Data Points		
	Unprocessed	*Processed*	*Removed*
A-4	120	113	7
A-6	405	390	15
A-7-6	510	492	18
Total	1035	995	40

However, there was a notable shift in Mr, with the highest value dropping from 72.91 MPa to 52.65 MPa, as well as a considerable stabilization in standard deviation, skewness, and kurtosis. This means that the skewness and extreme values were significantly reduced, resulting in more stable and consistent Mr values in the dataset, as evident from Table II and Figure 5.

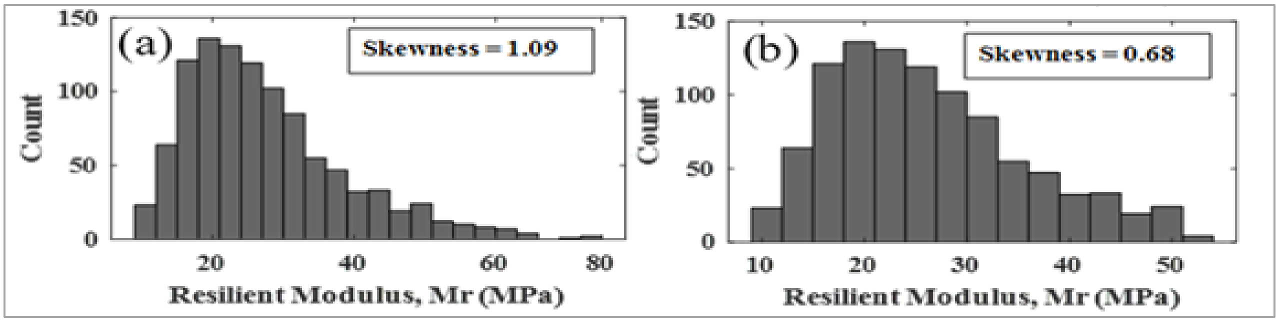

Figure 5: Distribution of resilient modulus (Mr) (a) before and (b) after outlier removal.

This improvement is verified by the boxplots in Figure 6, which indicate a considerable reduction in the number and extent of outliers following preprocessing. The cleaned dataset exhibits a more consistent spread with a largely unchanged median. Furthermore, the normal data range is comparatively cleaner and compact, indicating improved data quality and suitability for model training.

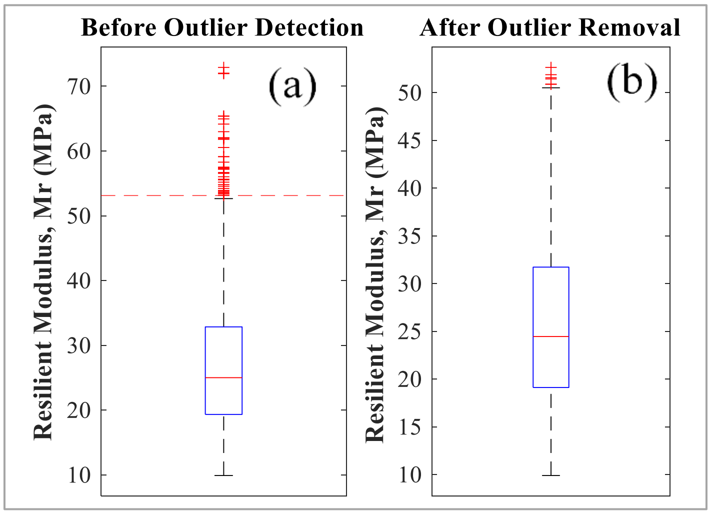

Figure 6: Outlier comparison of resilient modulus (Mr) values (a) before and (b) after IQR Outlier Preprocessing.

The findings of correlation analysis in Figure 7 shows that some inputs, such as LL and PI, or MC and DD, are highly correlated. This is expected behavior according to principles of soil mechanics, as the maximum dry density (MDD) of soils decreases after moisture content (MC) increases beyond optimum moisture content (OMC) levels, thus justifying the highly negative and inverse correlation between DD and MC. Similarly, LL and PI are strongly correlated, as the plasticity index (PI) is defined as PI=LL-PL, which explains their high positive correlation. However, most of the remaining input variables exhibited weak to moderate correlation with one another.

Nonetheless, all inputs were retained, since a neural network can effectively handle correlated inputs, and the aim of this study was reliable predictions, rather than reducing the number of variables.

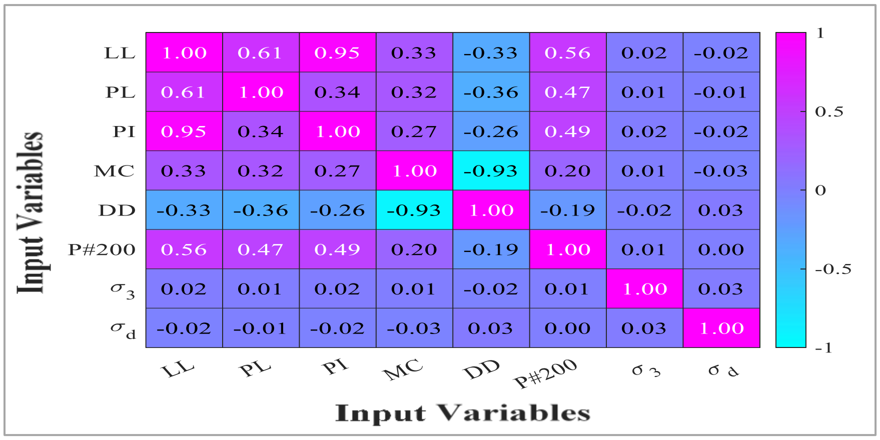

Figure 7: Correlation heatmap of processed dataset input variables.

L. Dataset Splitting Verification

Table IV demonstrates the distribution of soil types throughout the training, validation, and test sets. Every subset had almost equal shares of each soil class, indicating that the stratified divide was effective. Table V shows that the target variable (Mr) has near similar mean, spread, and minimum-maximum values across all three sets. Overall, the consistency in both soil type proportions and target variable statistics across all subsets indicates that the stratification process was successfully implemented.

Table IV. Distribution of soil classes across training, validation, and testing subsets.

Soil Type	Training Subset Count	Validation Subset Count	Testing Subset Count	Training Subset Proportion	Validation Subset Proportion	Test Subset Proportion
A-4	68	24	21	11.41	11.88	10.66
A-6	233	79	78	39.09	39.11	39.59
A-7-6	295	99	98	49.50	49.01	49.75

Table V: Descriptive Statistics of Target Variable (Mr) across Data Subsets.

Dataset	Resilient Modulus (Mr) Statistics Across Subsets			
	Mean (MPa)	*Std (MPa)*	*Min (MPa)*	*Max (MPa)*
Training	26.11	9.33	9.90	51.89
Validation	26.22	9.62	10.87	52.65
Testing	26.13	9.28	10.99	50.90

M. Bayesian Optimization Results

Figure 8 shows the convergence behavior of the Bayesian optimization session. The objective function (validation MAE) decreased noticeably during the initial trials, especially around the first 10 trials, before stabilizing shortly after the 60th trial as the optimization progressed, indicating effective exploration followed by convergence. After this stage, no noticeable performance improvement was detected, indicating that the optimization process had effectively explored and exploited the available hyperparameter search and discovered near-optimal hyperparameters.

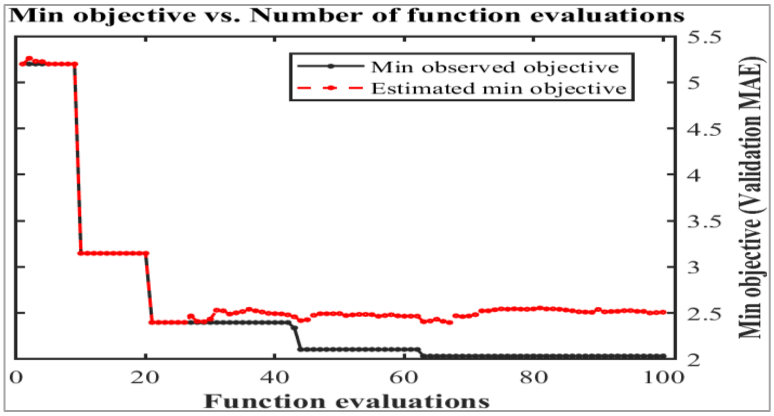

Figure 8: Convergence history of Bayesian Optimization (BO) showing validation MAE reduction across trials.

Figure 9 shows the variance in performance measures or metrics (RMSE, R^2, MAPE, and MAE) over all trials. The best-performing model configuration with the lowest validation MAE was obtained at the 64th iteration. It can be observed from Figure 9 that the optimal DNN model hyperparameter settings at the 64th iteration yield not only the lowest validation MAE, but also the lowest Validation RMSE and MAPE, along with the highest corresponding validation R^2, as compared to all other hyperparameter settings tested by the BO.

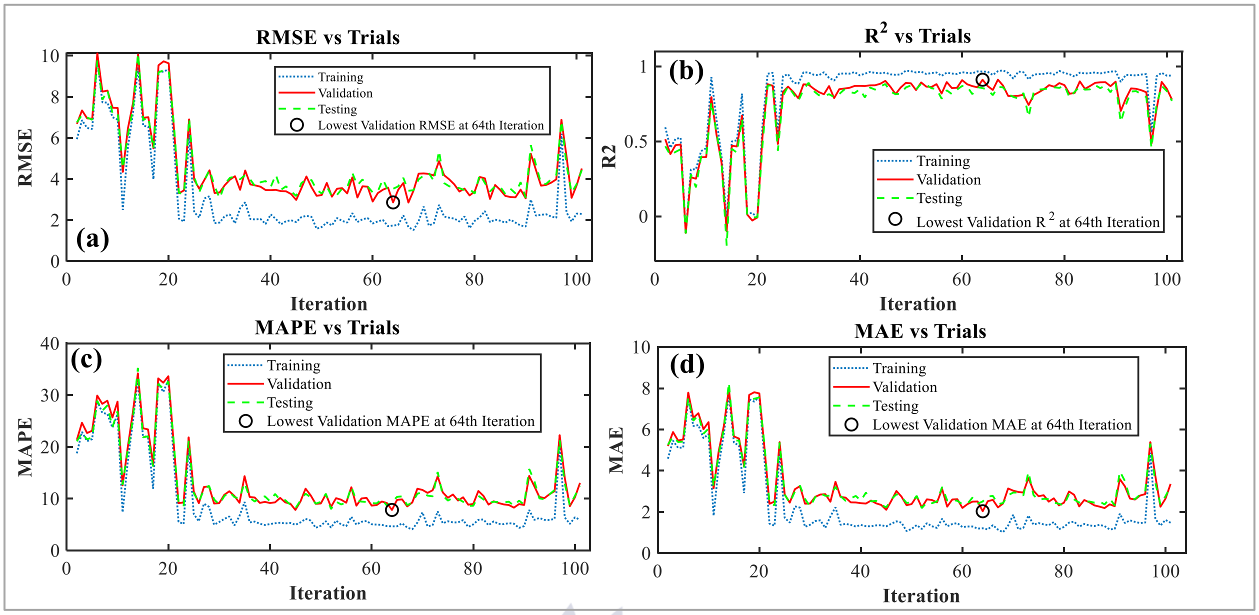

Figure 9: Variation of training, validation and testing performance metrics (a)RMSE (b)R^2 (c) MAPE and (d) MAE across Bayesian optimization trials.

Figure 9 further demonstrates the effectiveness of BO, because It can be observed that as the iterations proceed, the BO's surrogate model keeps updating, leading to more optimal configurations with lower validation MAE, RMSE, and MAPE and higher corresponding validation R^2

Table VI summarizes the optimal set of hyperparameters, corresponding to the optimal DNN model discovered via Bayesian optimization. These hyperparameter settings belong to the trial with the lowest validation error.

Table VI: Summary of Optimized DNN Hyperparameters select using Bayesian Optimization

Component / Hyperparameter	Value	Component / Hyperparameter	Value
Input layer neurons	11 (Equal to Inputs)	Output layer neurons	1 (Equal to Output)
Hidden layers	3	Output activation	Linear
Neurons per hidden layer	27	Optimizer	Adam
Activation function	ReLU	Learning rate	0.00087284

N. Optimal DNN Model Architecture and Performance Evaluation

Figure 10 and Table VII demonstrate that the DNN model performed decently across all datasets. The model achieved R^2 values greater than 0.90 for training and validation, and above 0.80 for testing. The error was quite low across all datasets, with all RMSE and MAE below 4 MPa and 3 MPa, respectively. MAPE values were below 10% across all subsets, which means that the model's prediction error is less than 10% of the actual Mr value. Overall, the model generalizes effectively on a global level, and performance decreased only slightly from training to testing.

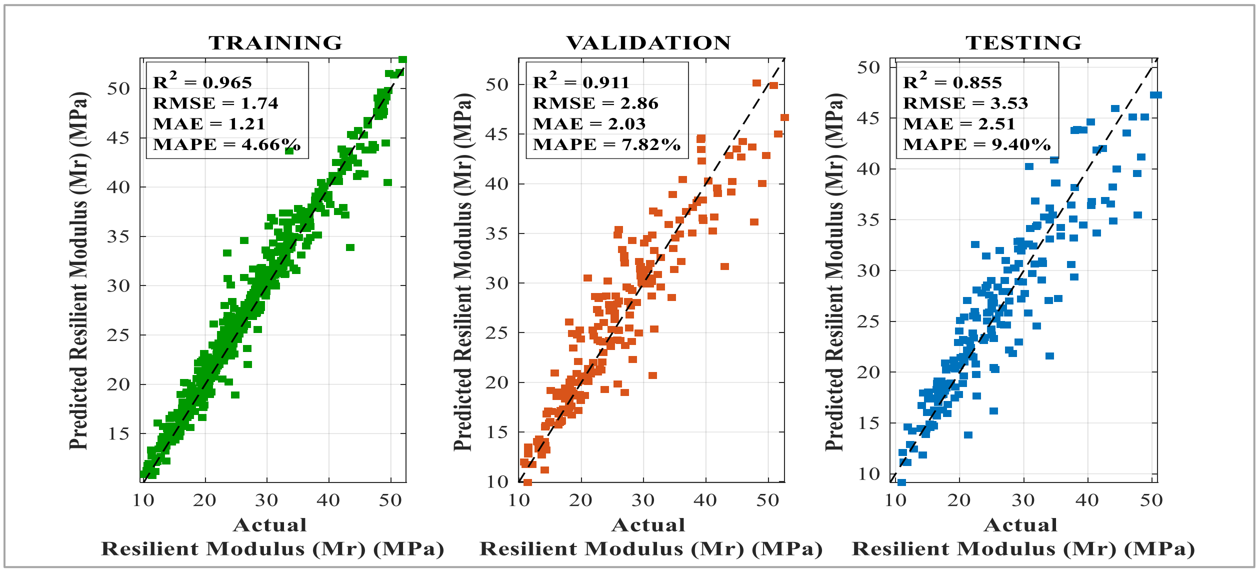

Figure 10: Predicted versus actual resilient modulus values for (a) training, (b) validation, and (c) testing datasets.

Table VII: Performance Evaluation Of the developed Model Across subsets at Global and Soil Level

Dataset	Level	Category	R^2	MAE	RMSE	MAPE
Training	Global	ALL	0.97	1.21	1.74	4.66
	Soil	A-4	0.95	1.36	2.05	4.71
		A-6	0.96	1.12	1.92	4.38
		A-7-6	0.97	1.13	1.56	4.90
Validation	Global	ALL	0.91	2.03	2.86	7.82
	Soil	A-4	0.89	2.87	3.85	8.80
		A-6	0.85	2.57	3.74	9.51
		A-7-6	0.89	2.40	3.15	10.22
Testing	Global	ALL	0.85	2.51	3.53	9.40
	Soil	A-4	0.71	3.37	4.32	11.33
		A-6	0.85	2.96	3.73	10.90
		A-7-6	0.86	2.45	3.41	9.71

When the model's performance was analyzed at the soil level individually, the model performed quite consistently. On the test set, the A 4 soil group exhibited somewhat lower performance with R^2 = 0.71, whereas A 6 and A 7 6 soils provided comparatively more reliable and stable predictions. Nonetheless, the model demonstrated reliable predictive capability across all soil categories, and other than slight variations in error, specifically MAPE and predictive capability (R^2), the error and performance of the model at the soil level remained within close agreement as evident from Table VII . Furthermore, Figure 10 presents the predicted and actual resilient modulus (Mr) values for the training, validation, and test sets. It is quite evident from Figure 10 that the data points closely adhere to the 1:1 reference line, suggesting excellent agreement between projected and measured values. The dispersion in predictions rises somewhat from training to testing, which corresponds to the observed drop in performance indicators. Moreover, across all three sets, the dispersion becomes somewhat more evident at moderate to higher values compared to lower values, suggesting that the model's predictive capability may struggle with moderate to higher Mr values.

The training and validation loss curves shown in Figure 11 indicate stable convergence of the model, with both losses decreasing rapidly and remaining close throughout training, suggesting minimal overfitting.

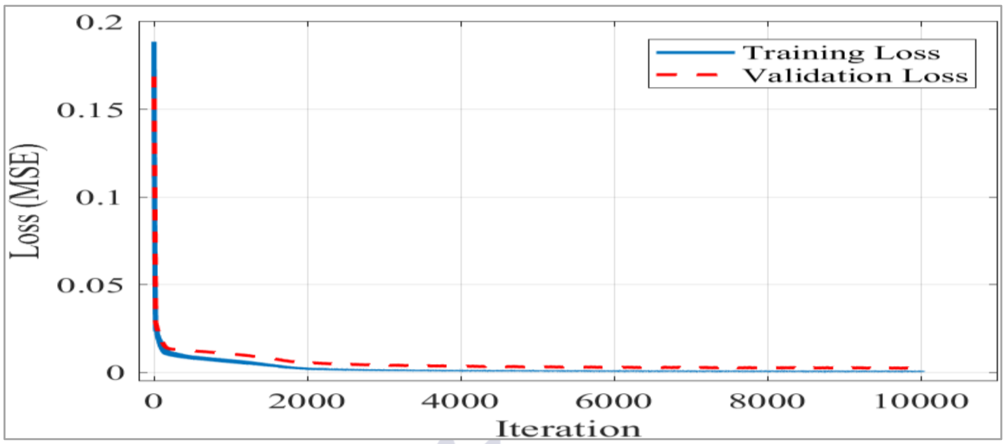

Figure 11: Training and validation loss curves of the optimized deep neural network DNN model.

Finally, for completeness, the architecture of the optimal DNN model is presented in Figure 12, and the corresponding hyperparameter details of the model are summarized in Table VI.

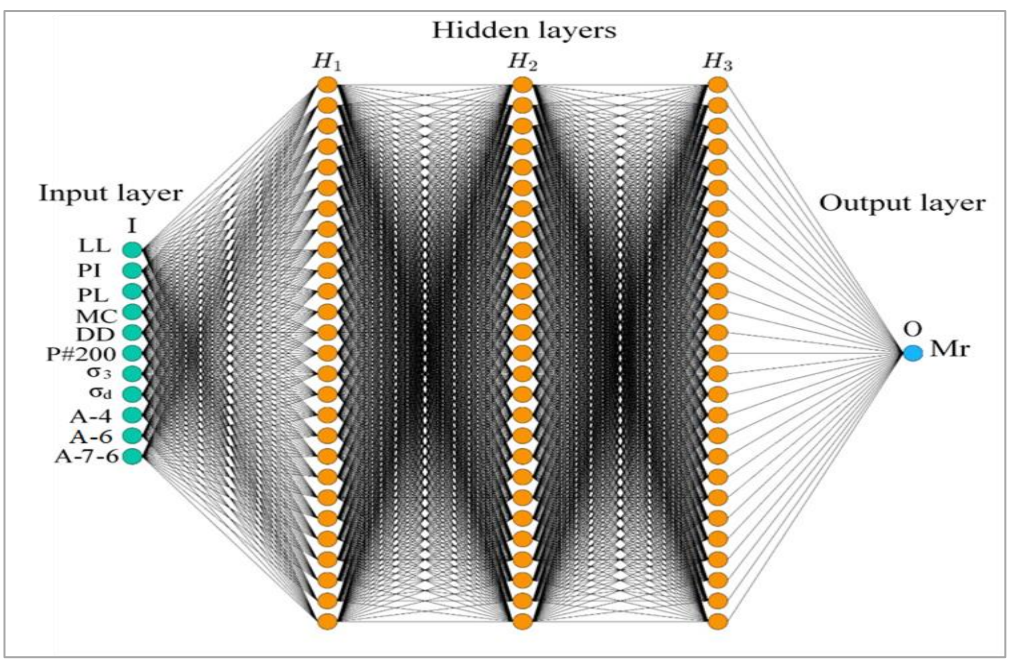

Figure 12: Architecture of the optimized deep neural network (DNN) model.

O. Residual Analysis Results

The residuals for the test set are shown in Figure 13. Most residuals are close to zero, indicating that the model's predictions are typically unbiased and not consistently too high or too low. There is a noticeable slight increase in error magnitude dispersion at moderate to higher Mr values, with both positive and negative errors present in all soil types. This behavior is consistent with earlier findings from Figure 10. Larger errors are uncommon and are often associated with larger Mr value predictions. Overall, the residual spread for A-4 soil is comparatively higher and more noticeable, with A-6 soil showing a similar well pronounced pattern of dispersion. On the other hand, A-7-6 soil as a whole exhibit a compact residual pattern.

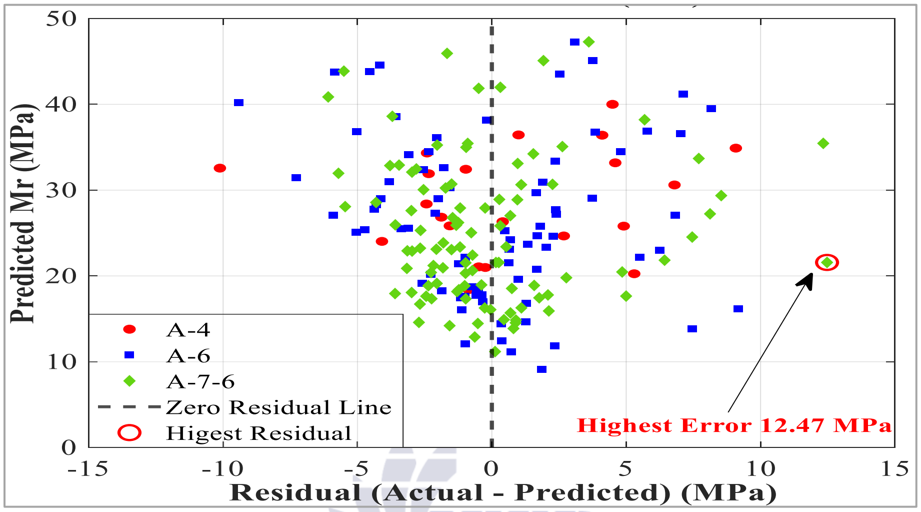

Figure 13: Residual distribution of the optimized deep neural network (DNN) model for the testing dataset.

Figure 14 shows the ten (10) largest absolute errors. The largest one is around 12.47 MPa, corresponding to A 7–6 soil. Moreover, several of these highest absolute errors correspond to A–7–6 soils, followed by comparatively lower values associated with A-4 and then A-6 respectively. This shows that the majority of the prediction error is caused by a small number of data points.

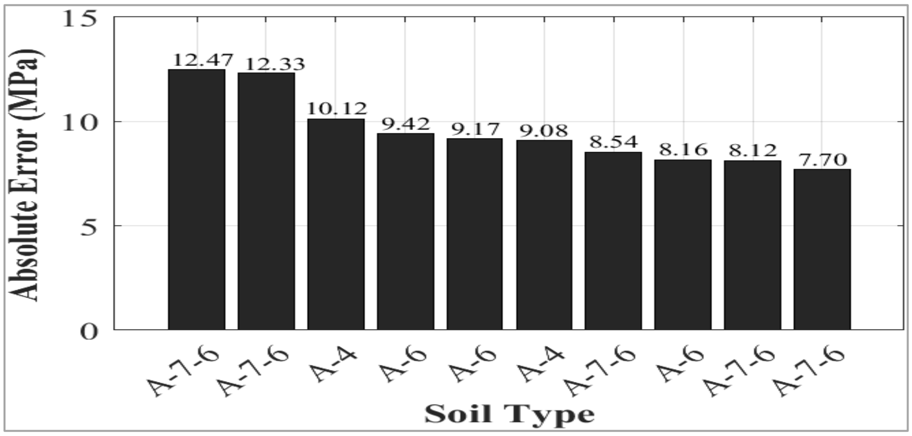

Figure 14: Largest absolute prediction errors observed in the testing dataset.

As presented in Figure 15, A-4 soils have the greatest MAE, followed by A-6 and A-7-6 soils, confirming the comparatively lower predictive performance for A-4 soil observed earlier based on findings in Table VII. Overall, the residual analysis indicates that the model is fairly consistent, with most errors clustered near zero and only a limited number of higher-error cases.

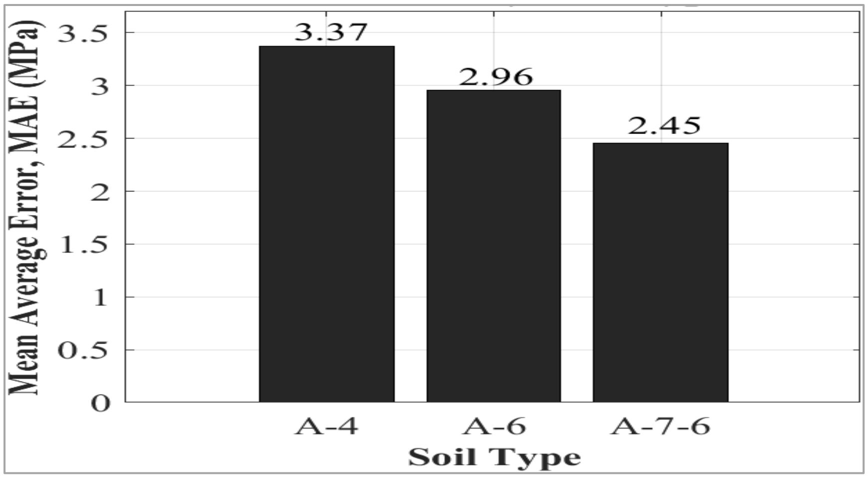

Figure 15. Mean absolute error (MAE) comparison among different soil classes.

P. Sensitivity Analysis Results

A parametric sensitivity analysis is presented in Figure 16, and a few things are quite evident. The plasticity of the soils (PI), σd, and Moisture content (MC) had the largest effect at 17.4%, 16.8% and 15% respectively. P#200, LL and PL were in the middle with moderate influence. σ_3 and Dry density (DD) were the least influent factors. Overall, the pattern is that plasticity, deviator stress state and moisture content of the soil are the most important variables for predicting the resilient modulus based on our developed DNN model.

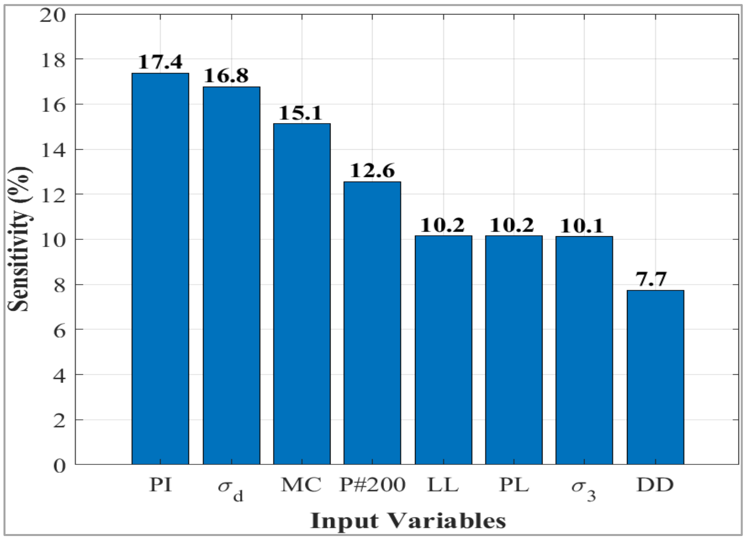

Figure 16: Sensitivity analysis of input variables influencing resilient modulus prediction.

Q. Limitations of the DNN model and Guidelines for Use

It is recommended that the developed DNN model should be utilized for making predictions with data which is within the training range of our data. Predictions made for values outside of the training range may be unreliable. It can thus be noted that, in order to get correct results, all the input parameters should stay within the bounds of the training set.

Prior to using the model for predictions with new data, the new input data should be normalized using the same minimum and maximum values used for the training dataset of the DNN. Similarly, meaningful output predictions can only be obtained when the predicted outputs are denormalized using the corresponding minimum and maximum output values from the training dataset.

The effectiveness of the model is also dependent on the quality and distribution of training data. Prediction accuracy can be reduced in cases where the distribution of the data contains too much noise, missing values, or is too far from the distribution of the data used for the training set. Hence proper preprocessing and verification of the new input data is recommended prior to using the model in practice.

Conclusion

The Bayesian Optimization (BO) process was able to successfully determine an optimal set of DNN hyperparameters without manual trial and error tuning. The best DNN model, determined by Bayesian Optimization (BO), consisted of 3 hidden layers with 27 neurons in each layer, utilizing the ReLU activation function and the Adam optimizer, and was trained for approximately 2500 epochs.

The optimized BO-DNN model demonstrated high prediction performance on both training and validation sets as well as the testing set. The model achieved R^2 value as high as approximately 0.97, 0.91, and 0.86 for the training, validation, and testing sets, respectively, while maintaining low prediction error when tested on unseen data, with both test MAE of 2.51MPa and test RMSE of 3.53MPa. In addition, all datasets had MAPE values below 10%, ensuring that all predictions were accurate. In the case of soil-specific performance, the model exhibited moderate level of performance for A-4 soil with testing R^2 0.71, while the performance was comparatively more accurate and reliable for A-6 and A-7-6 soils. The residual analysis revealed that most prediction errors were near zero, and only a few were larger errors, with only a limited number of larger errors mainly occurring at moderate to higher Mr values.

According to the sensitivity analysis, the DNN model regarded the soil's plasticity in terms of plasticity index (PI), stress state in terms of its deviator stress state (σd) and moisture content (MC) as the most influential parameter affecting resilient modulus prediction, followed by gradation such as P#200 and individual soil state explaining Atterberg limits like LL and PL. The confining pressure (σ_3) and the dry density (DD) was the least influential.

In conclusion, the results suggest that BO-DNN framework can be a practical and reliable alternative to expensive and time-consuming lab testing for estimating resilient modulus (Mr) of subgrade soils, as long as the predictions stay within the range of data used to train the model.

Acknowledgment

The authors would like to thank University of Engineering and Technology (UET), Peshawar, for providing the facilities and support required for this research. The authors are also grateful to their colleagues and peers for their guidance and encouragement throughout the course of this work. The support provided through the UET Peshawar Endowment Fund Scholarship Program is sincerely acknowledged.

Author Contributions

The authors contributed equally to the conception, methodology, analysis, and writing of this study.

Conflicts of Interest

There are no conflicts to declare.

REFERENCES

[1] K. Riaz and N. Ahmad, "Predicting resilient modulus: A data driven approach integrating physical and numerical techniques," Heliyon, vol. 10, no. 3, p. e25339, Feb. 2024, doi: 10.1016/j.heliyon.2024.e25339.

[2] H. J. Kim, Y.-H. Byun, J.-S. Lee, H. Seo, and D.-J. Kim, "Machine learning–based estimation of subgrade resilient modulus using sensor signals from in-situ modulus detector," Transp. Geotech., vol. 60, p. 101995, May 2026, doi: 10.1016/j.trgeo.2026.101995. https://doi.org/10.1016/j.trgeo.2026.101995

[3] Z. Yang, J. Sun, Y. Zhang, J. Liu, E. Oh, and Z. Ma, "A Systematic Evaluation of the Empirical Relationships Between the Resilient Modulus and Permanent Deformation of Pavement Materials," Buildings, vol. 15, no. 5, p. 663, Jan. 2025, doi: 10.3390/buildings15050663.

[4] A. J. Taylor, "Mechanistic Characterization of Resilient Moduli for Unbound Pavement Layer Materials," M.S. thesis, Dept. of Civil Engineering, Auburn University, Auburn, AL, USA, 2008. [Online]. Available: https://etd.auburn.edu/handle/10415/1159

[5] K. Wang and Y. Zhuang, "Characterizing the permanent deformation Response-Behavior of subgrade material under cyclic loading based on the shakedown theory," Constr. Build. Mater., vol. 311, p. 125325, Dec. 2021, doi: 10.1016/j.conbuildmat.2021.125325. https://doi.org/10.1016/j.conbuildmat.2021.125325

[6] M. I. Ozkaynak and Y. Yilmaz, "Prediction of resilient modulus with pre-post experimental data of undisturbed subgrade soils using machine learning algorithms," Transp. Geotech., vol. 49, p. 101396, Nov. 2024, doi: 10.1016/j.trgeo.2024.101396. https://doi.org/10.1016/j.trgeo.2024.101396

[7] M. M. E. Zumrawi and M. Awad, "Estimation of Subgrade Resilient Modulus from Soil Index Properties," in Proc. 19th Int. Conf. on Construction and Civil Engineering (ICCCE 2017), London, U.K., Sep. 21–22, 2017, doi: 10.5281/zenodo.1132477. [Online]. Available: https://publications.waset.org/10008058/estimation-of-subgrade-resilient-modulus-from-soil-index-properties

[8] D. H. Agustina and A. Zainorabidin, "Evaluation of resilient modulus and unconfined compressive strength of subgrade," E3S Web Conf., vol. 156, p. 01009, 2020, doi: 10.1051/e3sconf/202015601009.

[9] Y. F. Al-Dulaimi, A. M. Awed, A. Gabr, and S. EL-Badawy, "Predicting Resilient Modulus of Unbound Granular Base/Subbase Material," [Online]. Available: https://mej.researchcommons.org/home/vol47/iss2/1

[10] W. M. de Souza, A. J. A. Ribeiro, and S. H. de A. Barroso, "Estimating the resilient modulus of subgrade materials using visual inspection," Transportes, vol. 30, no. 3, pp. 2738–2738, Dec. 2022, doi: 10.14295/transportes.v30i3.2738.

[11] S. Khoshnevisan, M. Norouzi, and L. Sadik, "Use of Machine Learning Methods to Obtain a Reliable Predictive Model for Resilient Modulus of Subgrade Soil," [Online]. Available: https://docs.lib.purdue.edu/jtrp/1876

[12] A. A. Araya, M. Huurman, A. A. A. Molenaar, and L. J. M. Houben, "Investigation of the resilient behavior of granular base materials with simple test apparatus," Mater. Struct., vol. 45, no. 5, pp. 695–705, May 2012, doi: 10.1617/s11527-011-9790-1.

[13] C. Plati, M. Tsakoumaki, and A. Armeni, “Impact of Moisture Content on Resilient Modulus Predictions for Unbound Granular Materials Using Stress-Dependent Constitutive Models,” Transp. Infrastruct. Geotechnol., vol. 12, no. 6, p. 193, Aug. 2025, doi: 10.1007/s40515-025-00654-0.

[14] N. K. Farh, A. M. Awed, and S. M. El-Badawy, “Artificial Neural Network Model for Predicating Resilient Modulus of Silty Subgrade Soil,” Am. J. Civ. Eng. Archit., vol. 8, no. 2, pp. 52–55, May 2020, doi: 10.12691/ajcea-8-2-4.

[15] C. Plati and M. Tsakoumaki, “A Critical Comparison of Correlations for Rapid Estimation of Subgrade Stiffness in Pavement Design and Construction,” Constr. Mater., vol. 3, no. 1, pp. 127–142, Mar. 2023, doi: 10.3390/constrmater3010009.

[16] L. Camarena, “Using Artificial Intelligence to Estimate Nonlinear Resilient Modulus Parameters from Common Index Properties,” Transp. Res. Rec., Aug. 2021. [Online]. Available: https://journals.sagepub.com/doi/10.1177/03611981211023766

[17] A. Azam et al., “Modeling resilient modulus of subgrade soils using LSSVM optimized with swarm intelligence algorithms,” Sci. Rep., vol. 12, no. 1, p. 14454, Aug. 2022, doi: 10.1038/s41598-022-17429-z.

[18] C. C. Ikeagwuani, D. C. Nwonu, and C. C. Nweke, “Resilient modulus descriptive analysis and estimation for fine-grained soils using multivariate and machine learning methods,” Int. J. Pavement Eng., vol. 23, no. 10, pp. 3409–3424, Aug. 2022, doi: 10.1080/10298436.2021.1895993.

[19] A. R. P., “State-of-the-art review on predicting stabilized soil properties using artificial neural networks,” Mach. Learn. Data Sci. Geotech., vol. 2, no. 1, pp. 87–111, Mar. 2026, doi: 10.1108/MLAG-02-2025-0004.

[20] B. O. da Silva, M. M. de Queiroz, G. Oliveira, and G. J. C. Gomes, “Predicting resilient modulus for pavement design: a comprehensive review of artificial neural network applications,” Int. J. Pavement Eng., Nov. 2024, doi: 10.1080/10298436.2024.2426058.

[21] H. Liu, H. Su, L. Sun, and D. Dias-da-Costa, “State-of-the-art review on the use of AI-enhanced computational mechanics in geotechnical engineering,” Artif. Intell. Rev., vol. 57, no. 8, p. 196, Aug. 2024, doi: 10.1007/s10462-024-10836-w.

[22] A. Głuchowski, “Prediction of Resilient Modulus Value of Cohesive and Non-Cohesive Soils Using Artificial Neural Network,” Materials, vol. 17, no. 21, p. 5200, Jan. 2024, doi: 10.3390/ma17215200.

[23] J. Agunwamba, M. T. Tiza, and F. Okafor, “An appraisal of statistical and probabilistic models in highway pavements,” Turk. J. Eng., vol. 8, no. 2, pp. 300–329, Apr. 2024, doi: 10.31127/tuje.1389994.

[24] N. Baldo, M. Miani, F. Rondinella, E. Manthos, and J. Valentin, “Road Pavement Asphalt Concretes for Thin Wearing Layers: A Machine Learning Approach towards Stiffness Modulus and Volumetric Properties Prediction,” Period. Polytech. Civ. Eng., vol. 66, no. 4, pp. 1087–1097, Sep. 2022, doi: 10.3311/PPci.19996.

[25] J. Khatti and K. S. Grover, “Determination of Suitable Hyperparameters of Artificial Neural Network for the Best Prediction of Geotechnical Properties of Soil,” Int. J. Res. Appl. Sci. Eng. Technol., vol. 10, no. 5, pp. 4931–4961, May 2022, doi: 10.22214/ijraset.2022.43662.

[26] M. Miani et al., “Bituminous Mixtures Experimental Data Modeling Using a Hyperparameters-Optimized Machine Learning Approach,” Appl. Sci., vol. 11, no. 24, p. 11710, Dec. 2021, doi: 10.3390/app112411710.

[27] K. Sandjak and M. Ouanani, "Bayesian optimization algorithm based support vector regression analysis for estimation of resilient modulus of crushed rock materials for pavement design," MATEC Web Conf., vol. 396, p. 05016, 2024, doi: 10.1051/matecconf/202439605016.

[28] M. Shahin, M. B. Jaksa, and H. Maier, "State of the art of artificial neural networks in geotechnical engineering," Electron. J. Geotech. Eng., vol. Bouquest08, pp. 1–26, 2008. [Online]. Available: https://hdl.handle.net/20.500.11937/45940

[29] L. Khawaja et al., "Development of machine learning models for forecasting the strength of resilient modulus of subgrade soil: genetic and artificial neural network approaches," Sci. Rep., vol. 14, no. 1, p. 18244, Aug. 2024, doi: 10.1038/s41598-024-69316-4.

[30] S. Hanandeh, A. Ardah, and M. Abu-Farsakh, "Using artificial neural network and genetics algorithm to estimate the resilient modulus for stabilized subgrade and propose new empirical formula," Transp. Geotech., vol. 24, p. 100358, Sep. 2020, doi: 10.1016/j.trgeo.2020.100358.

[31] X. Hu and P. Solanki, "Predicting Resilient Modulus of Cementitiously Stabilized Subgrade Soils Using Neural Network, Support Vector Machine, and Gaussian Process Regression," Int. J. Geomech., vol. 21, no. 6, p. 04021073, Jun. 2021, doi: 10.1061/(ASCE)GM.1943-5622.0002029.

[32] M. Tanyildizi, "Strength and resilient performance of expansive subgrades stabilized with apricot kernel shell ash," Sci. Rep., vol. 16, p. 17439, Apr. 2026, doi: 10.1038/s41598-026-48290-z.

[33] M. Tanyıldızı and İ. Gökalp, "Stabilization of expansive road subgrades with waste paper sludge: Resilient modulus, ANN and modeling approach," Transp. Geotech., vol. 52, p. 101552, May 2025, doi: 10.1016/j.trgeo.2025.101552.

[34] R. Polo-Mendoza, J. Duque, D. Mašín, E. Turbay, and C. Acosta, "Implementation of deep neural networks and statistical methods to predict the resilient modulus of soils," Int. J. Pavement Eng., vol. 24, no. 1, Art. no. 2257852, 2023, doi: 10.1080/10298436.2023.2257852.

[35] N. Kardani, A. Kumar, S. Kumar, O. Karr, and A. Bardhan, "A Deep Learning Approach for Modelling of Resilient Modulus of Compacted Subgrade Subjected to Freezing-Thaw Cycles and Moistures," Transp. Infrastruct. Geotechnol., vol. 11, no. 6, pp. 3805–3828, Dec. 2024, doi: 10.1007/s40515-024-00439-x.

[36] M. A. Benbouras, L. Sadoudi, and A. Leghouchi, "Prediction of the resilient modulus of subgrade soil using machine-learning techniques," Urban. Arhit. Constr., vol. 16, no. 1, pp. 87–104, Apr. 2025. [Online]. Available: https://uac.incd.ro/Art/v16n1a6.pdf

[37] N. Elshaboury, M. S. Yamany, S. Labi, and O. Smadi, "Enhancing local road pavement condition prediction using Bayesian-optimized ensemble machine learning and adaptive synthetic sampling technique," Int. J. Pavement Eng., vol. 25, no. 1, Art. no. 2365957, 2024, doi: 10.1080/10298436.2024.2365957.

[38] T.-G. Nguyen, D. Tran, and P. Nguyen, "Prediction of Concrete Compressive Strength Using Artificial Neural Network with Bayesian Optimization," Mater. Emerg. Technol. Sustain., vol. 01, Apr. 2025, doi: 10.1142/S3060932125500074.

[39] K. Sandjak and M. Ouanani, "A Novel Prediction Technique for the Resilient Modulus of Unbound Aggregates Combined XGBoost Algorithm with Bayesian Optimization," in ARPHA Proceedings, Pensoft Publishers, pp. 254–264, Oct. 2024, doi: 10.3897/ap.7.e0254.

[40] M. Xu, Y. Kang, S. Ma, and H. Zhang, “Subgrade Resilient Modulus Prediction with XGBoost Model Based on Bayesian Optimization,” J. Highw. Transp. Res. Dev., vol. 40, no. 11, pp. 51–60, Dec. 2024, doi: 10.3969/j.issn.1002-0268.2023.11.007.

[41] M. T. Cihan and P. Cihan, “Bayesian-Optimized Ensemble Models for Geopolymer Concrete Compressive Strength Prediction with Interpretability Analysis,” Buildings, vol. 15, no. 20, p. 3667, Jan. 2025, doi: 10.3390/buildings15203667.

[42] R. K. Tipu, A. Goyal, D. Singh, and A. K. A. Kumar, “Integrated deep learning and Bayesian optimization approach for enhanced prediction of high-performance concrete strength,” Asian J. Civ. Eng., vol. 26, no. 6, pp. 2371–2390, Jun. 2025, doi: 10.1007/s42107-025-01313-y.

[43] M. Hiçyılmaz, “Bayesian optimization-enhanced vision transformer for damage detection in steel truss structures using continuous wavelet transform analysis,” Structures, vol. 85, p. 111059, Mar. 2026, doi: 10.1016/j.istruc.2026.111059.

[44] M. Nasser, E. Assefa, S. M. Assefa, T. B. Kebede, C. C. Sachpazis, and L. Pantelidis, “Bayesian optimization for uncertainty-aware prediction of rainfall-induced deformation in embankment dams,” Sci. Rep., vol. 16, p. 17319, Apr. 2026, doi: 10.1038/s41598-026-46994-w.

[45] A. Shah, T. Thaker, V. Shukla, and P. Ranpura, “Efficient predictive modeling of resilient modulus in stabilized clayey soil using automated machine learning,” Constr. Build. Mater., vol. 442, p. 137678, Sep. 2024, doi: 10.1016/j.conbuildmat.2024.137678.

[46] Y. Liu, J. Ni, F. Zhang, E. Kravchenko, and V. Kamchoom, “Bayesian-informed DNN and ensemble learning for predicting soil water characteristic curves from easily measurable parameters,” Transp. Geotech., vol. 56, p. 101791, Jan. 2026, doi: 10.1016/j.trgeo.2025.101791.

[47] Y. Gao, G. Huang, Y. Li, J. Zhang, Z. Yang, and M. Wang, “The Data-Driven Homogenization of Mohr–Coulomb Parameters Based on a Bayesian Optimized Back Propagation Artificial Neural Network (BP-ANN),” Appl. Sci., vol. 13, no. 21, p. 11966, Nov. 2023, doi: 10.3390/app132111966.

[48] N. Baldo, J. Valentin, E. Manthos, and M. Miani, “Numerical Characterization of High Modulus Asphalt Concrete Containing RAP: A Comparison among Optimized Shallow Neural Models,” IOP Conf. Ser. Mater. Sci. Eng., vol. 960, no. 2, p. 022083, Dec. 2020, doi: 10.1088/1757-899X/960/2/022083.

[49] H. Li and J. Zhou, “Prediction on the Resilience Modulus of Roadbeds Based on Coupled Bayesian with XGBoost Models,” in 2024 5th International Conference on Computer Engineering and Application (ICCEA), Hangzhou, China, 2024, pp. 1719–1723, doi: 10.1109/ICCEA62105.2024.10604270.

[50] A. Mughees, M. Kamran, N. Mughees, A. Mughees, and K. Ejsmont, “New Appliance Signatures for NILM Based on Mono-Fractal Features and Multi-Fractal Formalism,” IEEE Access, vol. 12, pp. 108986–109000, Aug. 2024, doi: 10.1109/ACCESS.2024.3440168.

[51] S. J. S. Hakim, J. Noorzaei, M. S. Jaafar, M. Jameel, and M. Mohammadhassani, “Application of artificial neural networks to predict compressive strength of high strength concrete,” Int. J. Phys. Sci., vol. 6, no. 5, pp. 975–981, Mar. 2011, doi: 10.5897/IJPS11.023.

[52] K. C. Onyelowe et al., “Selected AI optimization techniques and applications in geotechnical engineering,” Cogent Eng., vol. 10, no. 1, p. 2153419, Dec. 2023, doi: 10.1080/23311916.2022.2153419.

[53] F. Shen, I. Jha, H. F. Isleem, W. J. K. Almoghayer, M. Khishe, and M. K. Elshaarawy, "Advanced predictive machine and deep learning models for round-ended CFST column," Sci. Rep., vol. 15, no. 1, p. 6194, Feb. 2025, doi: 10.1038/s41598-025-90648-2.

[54] N. G. Jesubalan, G. Thakur, and A. S. Rathore, "Deep neural network for prediction and control of permeability decline in single pass tangential flow ultrafiltration in continuous processing of monoclonal antibodies," Front. Chem. Eng., vol. 5, p. 1182817, Jul. 2023, doi: 10.3389/fceng.2023.1182817.

[55] M. Maurizi, C. Gao, and F. Berto, "Inverse design of truss lattice materials with superior buckling resistance," Npj Comput. Mater., vol. 8, no. 1, p. 247, Nov. 2022, doi: 10.1038/s41524-022-00938-w.

[56] S. Oktay, İ. Duru, H. Bakır, T. E. Tabaru, et al., "Deep learning and machine learning based highly accurate reflection prediction model for multi layers anti-reflection coatings," Opt. Quantum Electron., vol. 57, p. 101, Jan. 2025, doi: 10.1007/s11082-024-08006-x.

[57] T. S. Tran, B. Stitmannaithum, L. Van Hong Bui, and T.-T. Nguyen, "Data-driven prediction of the shear capacity of ETS-FRP-strengthened beams in the hybrid 2PKT–ML approach," Sci. Rep., vol. 13, no. 1, p. 19871, Nov. 2023, doi: 10.1038/s41598-023-47064-1.

[58] A. Rojas Zuniga, S. Bakhtiari, C. Aldrich, V. M. Calo, and M. Iannuzzi, "Predicting stress corrosion cracking in downhole environments: a Bayesian network approach for duplex stainless steels," Npj Mater. Degrad., vol. 9, no. 1, p. 122, Oct. 2025, doi: 10.1038/s41529-025-00646-y.

[59] Z. Abulawi, R. Hu, P. Balaprakash, and Y. Liu, "Bayesian Optimized Deep Ensemble for Uncertainty Quantification of Deep Neural Networks: a System Safety Case Study on Sodium Fast Reactor Thermal Stratification Modeling," Reliab. Eng. Syst. Saf., vol. 264, p. 111353, Dec. 2025, doi: 10.1016/j.ress.2025.111353.

[60] A. Yu, Y. Li, S. Li, and J. Gong, "Construction High Precision Neural Network Proxy Model for Ship Hull Structure Design Based on Hybrid Datasets of Hydrodynamic Loads," J. Mar. Sci. Appl., vol. 23, no. 1, pp. 49–63, Mar. 2024, doi: 10.1007/s11804-024-00388-4.

[61] D. Cui, L. Shi, and K. Gao, "Rapid construction of Rayleigh wave dispersion curve based on deep learning," Front. Earth Sci., vol. 10, p. 1084414, Jan. 2023, doi: 10.3389/feart.2022.1084414.